Clay Minerals (2022), **57**, 97–104
doi:10.1180/clm.2022.25

CAMBRIDGE UNIVERSITY PRESS

Article

Influence of zirconia on the sintering behaviour and mechanical properties of reaction-sintered mullite-based composite ceramics

Zhenying Liu[1,2,3]*, Nan Xie[1], Shouwu Huang[1], Hanxin Zhang[1], Chongmei Wu[1], Kai Cui[1], Yin Liu[1,2,3], Hongzheng Zhu[1], Jinbo Zhu[1,2] and Changguo Xue[1]

[1]School of Materials Science and Engineering, Anhui University of Science and Technology, Huainan 232001, Anhui, China; [2]State Key Laboratory of Mining Response and Disaster Prevention and Control in Deep Coal Mines, Anhui University of Science and Technology, Huainan 232001, Anhui, China and [3]Anhui International Joint Research Center for Nano Carbon-based Materials and Environmental Health, Anhui University of Science and Technology, Huainan 232001, Anhui, China

ABSTRACT

High-performance mullite-based composite ceramics were prepared successfully using natural kaolin and alumina as raw materials and ZrO_2 as an additive. The influence of sintering temperature and ZrO_2 content on the sintering behaviour and mechanical properties of zirconia-toughened mullite ceramics was studied systematically. With increasing sintering temperature from 1450°C to 1560°C, the primary phases of as-sintered composite ceramics were mullite and corundum with a small amount of ZrO_2, and the bulk density of the composite ceramics increased from 2.29 to 2.72 g cm^{-3}. Furthermore, the ZrO_2 phase transition promoted transgranular fracture, and ZrO_2 grains were pinned at the grain boundaries, thereby enhancing the mechanical strength of the composite ceramics. Moreover, the AZS12 sample, with 12 wt.% ZrO_2 and sintered at 1560°C, had the greatest flexural strength and fracture toughness of 91.6 MPa and 2.47 MPa $m^{-1/2}$, respectively. Adding ZrO_2 to the composite ceramics increased their flexural strength by ~37.6%.

Keywords: alumina, kaolin, mullite-based composite ceramics, phase transition, zirconia-toughened mullite ceramics, ZrO_2

(Received 29 May 2022; revised 17 September 2022; Accepted Manuscript online: 6 October 2022; Associate Editor: M. Dondi)

Mullite is the only stable binary phase in the Al_2O_3–SiO_2 system at atmospheric pressure, and it is often present in the form of $3Al_2O_3{\cdot}2SiO_2$. Mullite ceramics are promising materials for industrial applications due to their excellent infrared transmission properties, good dielectric properties and thermal stability in high-temperature environments (Schneider *et al.*, 2008; Yu *et al.*, 2018; Li *et al.*, 2021; Romero *et al.*, 2021). In addition, mullite is also a critical matrix material for ceramic-based composites (Li *et al.*, 2017). For instance, mullite–corundum composite ceramics are functional ceramics with superior properties to pure corundum and mullite. Therefore, they have become suitable candidates for high-tech applications, such as in aerospace applications and high-temperature engines (Wu *et al.*, 2021b, 2021c).

Mullite is rare in nature and typically is prepared *via* heat treatment of Al–Si compounds at high temperatures according to mullite stoichiometry (Yuan *et al.*, 2022). The synthesis of mullite ceramics *via* pure raw materials is costly and requires high-temperature sintering. In recent years, some scholars have proposed novel processes for synthesizing mullite from mineral raw materials at low cost. For example, Alves *et al.* (2016) prepared mullite ceramics using a mixture of clay and kaolin waste *via* a reaction sintering technique. Moreover, Zhang *et al.* (2019) synthesized high-porosity mullite ceramics using kaolin as the raw material.

The decomposition of kaolin to form mullite also yields cristobalite (Sainz *et al.*, 2000; Sahnoune *et al.*, 2013; Aswad *et al.*, 2021), which transforms into an amorphous phase at high temperatures and impacts the mechanical properties of mullite composite ceramics negatively. To improve the mechanical strength and fracture resistance of mullite composite ceramics, some recent papers have focused on the modification of mullite through the introduction of secondary phases (Ji *et al.*, 2013; Mahmood *et al.*, 2017; Qian *et al.*, 2020; Qin *et al.*, 2020; Sarker *et al.*, 2022). Some agents, such as Al_2O_3 (Wu *et al.*, 2016), ZrO_2 (Sistani *et al.*, 2019) and SiC (Jing *et al.*, 2014), have been employed as secondary phases to reinforce mullite ceramics. The introduced Al_2O_3 reacts with excess cristobalite to form secondary mullite crystals (Bella *et al.*, 2021). Simultaneously, mullite–corundum composite ceramics can also be prepared. Generally, the presence of ZrO_2 promotes phase transformation toughening, which is achieved through the consumption of external energy *via* the phase transformation of ZrO_2 (t-ZrO_2 → m-ZrO_2, where t denotes the tetragonal phase and m denotes the monoclinic phase; Mazzei & Rodrigues, 2000). For instance, Wu *et al.* (2021a) prepared Al_2O_3–mullite–ZrO_2–SiC composite ceramics with excellent flexural strength using kaolin, α-Al_2O_3 and ZrO_2 as the raw materials, and the retention range of the flexural strength increased by 13.63% after 30 thermal-shock cycles. Serragdj *et al.* (2018) prepared mullite–zirconia composite ceramics successfully using kaolin, feldspar and quartz as the raw materials and introduced ZrO_2 as an additive to improve their mechanical strength. ZrO_2 plays a prominent role in strengthening ceramic materials; in addition, the sintering parameters can be

*Email: zyliu@aust.edu.cn

Cite this article: Liu Z *et al* (2022). Influence of zirconia on the sintering behaviour and mechanical properties of reaction-sintered mullite-based composite ceramics. *Clay Minerals* **57**, 97–104. https://doi.org/10.1180/clm.2022.25

© The Author(s), 2022. Published by Cambridge University Press on behalf of The Mineralogical Society of Great Britain and Ireland

https://doi.org/10.1180/clm.2022.25 Published online by Cambridge University Press

altered to tune the mechanical properties of ceramic materials (Prochazka *et al.*, 1983; Miranzo *et al.*, 1985; Yuan *et al.*, 1986; Koyama *et al.*, 1994, 1996). Therefore, it is necessary to further explore the effects of ZrO_2 on the sintering behaviour and mechanical properties of mullite-based composite ceramics.

The current study utilizes kaolin and Al_2O_3 as raw materials and introduces ZrO_2 as an additive to fabricate mullite-based composite ceramics *via* solid-state reaction sintering. Moreover, the influences of ZrO_2 content and sintering temperature on the bulk density, phase composition, microstructure and mechanical properties of these composite ceramics is studied systematically. In particular, the ZrO_2-assisted toughening mechanism of mullite-based ceramics is investigated in detail.

Experimental

Raw materials

Kaolin (dark yellow, $d_{50} = 11.2$ μm, Anhui Jinyan Kaolin Technology Co. Ltd, China) and alumina (white, Al_2O_3, analytically pure, Xilong Scientific Co. Ltd, China) powders were used as starting materials. Zirconia (white ZrO_2, purity >99%, Tianjin Fuchen Chemical Reagent Factory, China) was used as an additive and magnesium oxide (white MgO, purity >99.9%, Sinopharm Chemical Reagent Co. Ltd, China) was used as a sintering aid. The chemical composition of kaolin was determined using X-ray fluorescence (XRF) spectroscopy (Table 1). The X-ray diffraction (XRD) trace of the kaolin is presented in Fig. S1. The main crystalline phases of kaolin are kaolinite ($Al_4(Si_4O_{10})(OH)_8$, PDF #78-2109) and quartz (SiO_2, PDF #82-511). The material characterization and detailed experimental procedures can be provided in the Supplementary Materials.

Composite preparation and characterization

The starting materials were mixed for 1 h using a planetary ball mill according to the desired proportions (Table S1). Then, polyvinyl alcohol solution (5 wt.%) was used as a wet granulation binder. The mixtures were pressed into the desired green bodies (cylindrical samples: Φ15 mm × 5 mm, rectangular samples: 40 mm × 40 mm × 5 mm) under a uniaxial pressure of 20 MPa. After being dried at 100°C for 24 h, the samples were heated in a muffle furnace at 1450°C, 1500°C, 1520°C, 1540°C and 1560°C for 3 h, with a heating rate of 5°C min^{-1}. The sintered samples were labelled as AZS0, AZS3, AZS6, AZS9 and AZS12 corresponding to the ZrO_2 contents of 0, 3, 6, 9 and 12 wt.%, respectively (Table S1).

The bulk density and apparent porosity of the as-sintered ceramics were measured using the Archimedes method, as reported elsewhere (Ma *et al.*, 2010). The as-sintered ceramic phase compositions were examined using an X-ray diffractometer (Cu-*K*α radiation, λ = 0.154186 nm, Smartlab SE, Japan) at 30 mA and 40 kV. The scan speed was 5° min^{-1}, the scanning step was 0.02° and the lattice parameters and phase contents were calculated using *Jade 6.5* software based on the XRD results (Peng & Qin, 2019) and PDF database (PDF2-2004). The phase-transformation process and thermal decomposition during heat treatment were investigated using a thermal analyser (thermogravimetry-differential scanning calorimetry (TG-DSC), STA 409, Netzsch, Germany). The ceramics were heated from room temperature to 1100°C at a heating rate of 10°C min^{-1} in air. The prepared samples were gold-coated, and the microstructures of the fractured surfaces of the as-sintered ceramics were observed using a scanning electron microscope (SEM; Hitachi S4800, Japan) equipped with an energy-dispersive spectrum (EDS) analyser. The flexural strength and fracture toughness of the as-sintered ceramics were analysed using a ceramic bending strength tester (WDW-50, Kaiqiangli, China). The flexural strength was measured using a three-point bending method (Behera & Bhattacharyya, 2020). Similarly, the fracture toughness was measured using a single-edge notched beam method (Lian *et al.*, 2021a). The span length and loading speed were 30 mm and 0.5 mm min^{-1}, respectively. The calculation process for the mechanical properties of the ceramics is given in the Supplementary Materials.

Table 1. The chemical composition of the starting materials (wt.%).

Starting material	Al_2O_3	SiO_2	Fe_2O_3	TiO_2	K_2O	MgO	CaO	LOI
Kaolin	42.66	51.21	1.11	0.22	1.25	0.34	0.13	3.08
Al_2O_3	99.43	–	–	–	–	–	–	0.57

LOI = loss on ignition.

Results and discussion

Thermal analysis

Figure 1 shows the TG-DSC curves of the starting mixtures (kaolin, Al_2O_3) with and without 12 wt.% ZrO_2. The AZS0 sample presents endothermic and exothermic peaks at ~146°C and 296°C, respectively, in the range of room temperature to 400°C, corresponding to the loss of adsorbed water and the combustion of impurities. The overall mass loss was 2.94 wt.%. An indistinct endothermic peak appeared at 570°C, originating from the removal of structural water from kaolin and corresponding to a mass loss of 1.69 wt.%. At temperatures greater than 835°C, the ceramic mass increased slightly (0.81 wt.%) due to the oxidation of iron within the raw materials. Correspondingly, the TG-DSC curve of the sample with 12 wt.% zirconia is shown in Fig. 1b. Comparatively, the AZS12 sample exhibited a significant mass loss (8.63 wt.%) in three distinct stages (2.13 + 5.78 + 0.72 wt.%). The endothermic peak at 48°C corresponds to the evaporation of free water, while the exothermic peak at 283°C is related to the combustion of impurities. The second endothermic peak occurred at 495°C, which is attributed to the removal of lattice water from kaolin and its conversion into metakaolin. This process was similar to that observed in the AZS0 sample. At >800°C, there were significant differences between AZS0 and AZS12 samples. A clear exothermic peak appeared at 992°C in the curve of the AZS12 sample due to the initiation of mullite crystallization. These results are consistent with those of previous work (Mojumdar *et al.*, 2009; Vyazovkin *et al.*, 2011; Bella *et al.*, 2021).

Phase analysis

Figure 2 presents the XRD traces of the AZS6 ceramics after sintering at various temperatures. The main crystalline phase in the sample was mullite (PDF #74-2419) and the secondary crystalline phase was corundum (PDF #74-1081). In addition, small amounts of *t*-ZrO_2 (tetragonal, PDF #81-1314) and *m*-ZrO_2 phases (monoclinic, PDF #86-1450) were observed in the AZS6 ceramics. The intensity of the mullite peaks increased

https://doi.org/10.1180/clm.2022.25 Published online by Cambridge University Press

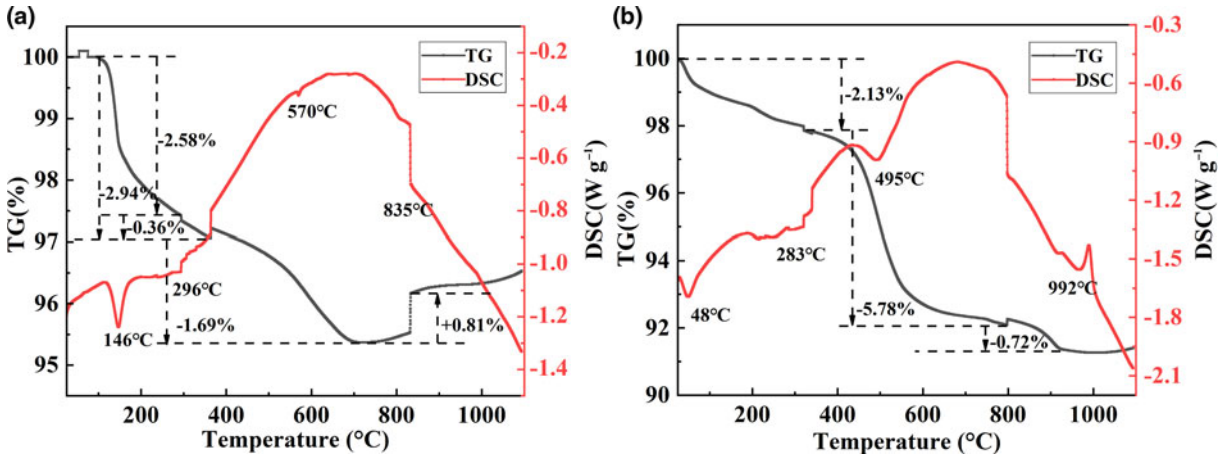

Fig. 1. TG-DSC curves of the composite ceramics with various amounts of ZrO_2: (a) AZS0 and (b) AZS12.

progressively when the sintering temperature increased to 1500°C. The increase in mullite content was related to the production of secondary mullite due to the added alumina reacting with the quartz by-product from the transformation of kaolin into mullite. The reactions can be described as in Equations 1 and 2 (Ptáček *et al.*, 2014; Liu *et al.*, 2019):

$$3(Al_2O_3 \cdot 2SiO_2)(\text{metakaolin}) \xrightarrow{968^\circ C} 3Al_2O_3 \cdot 2SiO_2\ (\text{mullite core}) + 4SiO_2 \quad (1)$$

$$3Al_2O_3 + 2SiO_2 \xrightarrow{>1300^\circ C} 3Al_2O_3 \cdot 2SiO_2\ (\text{secondary mullite}) \quad (2)$$

The XRD traces of the AZS ceramics sintered at 1560°C with various ZrO_2 contents are shown in Fig. 3a. In the absence of ZrO_2, the main crystalline phases were mullite and corundum. When the 3 wt.% ZrO_2 content was added, the characteristic peaks of *t*-ZrO_2 and *m*-ZrO_2 were detected in the AZS3 sample. When the ZrO_2 content was increased further to 6 wt.%, the intensity of the mullite peaks decreased slightly, suggesting that mullite may exist in the form of a solid solution. In addition, the intensity of the ZrO_2 peaks increased at ZrO_2 contents of >6 wt.% (Fig. 3b). Kwon & Jung (2022) suggested that the Al_2O_3–SiO_2 system describes sufficiently the coexistence of two phases at 1140 K (867°C) in the ternary phase diagram of Al_2O_3–SiO_2–ZrO_2. However, the Al_2O_3–SiO_2–ZrO_2 system cannot form ternary compounds, although it can still include mullite, Al_2O_3 and ZrO_2 in the liquid phase at 1823 K (1550°C). The corundum phase originated from the transformation of excessive Al_2O_3, whereas the introduction of ZrO_2 led to increased *t*-ZrO_2 contents. Based on phase transformation toughening, *t*-ZrO_2 can improve the mechanical properties of ceramics (Ma *et al.*, 2010; Lian *et al.*, 2021b; Weinberg *et al.*, 2021).

The lattice parameters of the mullite of as-sintered ceramics were calculated using *Jade 6.5* software from the XRD results (Table 2). The mullite was orthorhombic and the unit-cell parameters changed slightly with the addition of ZrO_2. More

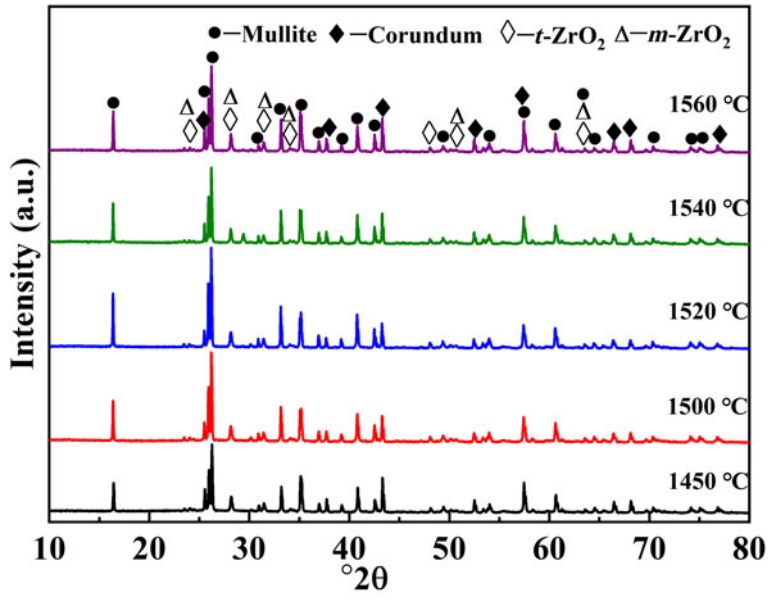

Fig. 2. XRD traces of AZS6 ceramics sintered at various temperatures.

https://doi.org/10.1180/clm.2022.25 Published online by Cambridge University Press

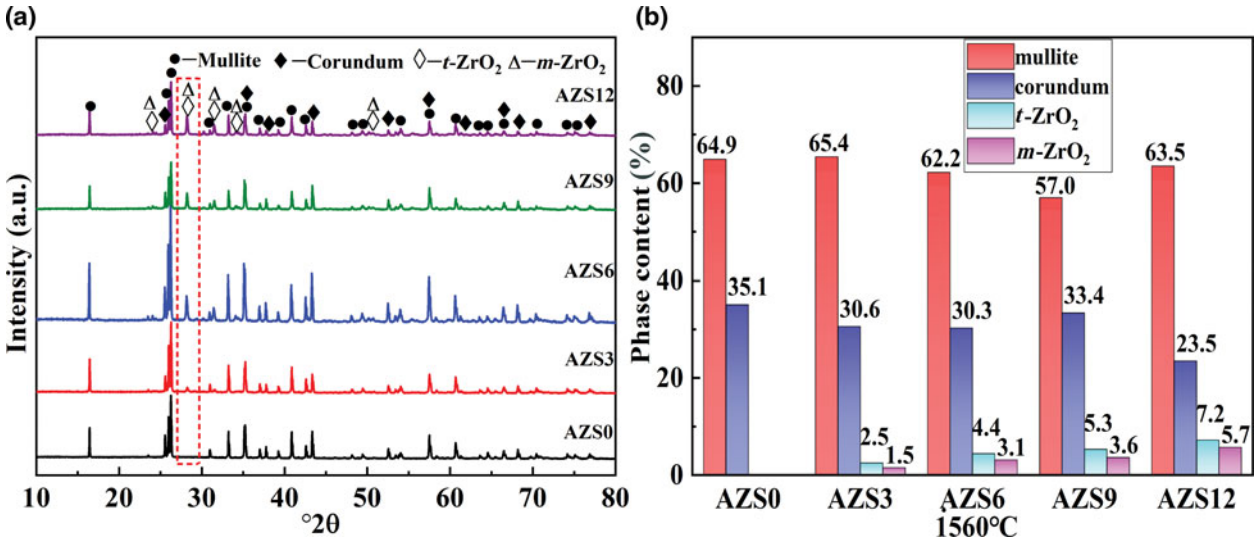

Fig. 3. (a) XRD traces and (b) phase contents of ceramics with various amounts of ZrO_2 after sintering at 1560℃.

Table 2. Lattice parameters of mullite in the composite ceramics with various amounts of ZrO_2 after sintering at 1560°C.

Sample	*a* (Å)	*b* (Å)	*c* (Å)	Crystal system	*V* (Å^3)
AZS0	7.549	7.681	2.884	Orthorhombic	167.23
AZS3	7.553	7.689	2.885	Orthorhombic	167.53
AZS6	7.564	7.699	2.895	Orthorhombic	168.56
AZS9	7.523	7.697	2.891	Orthorhombic	167.37
AZS12	7.557	7.689	2.885	Orthorhombic	168.62

specifically, the lattice parameters (*a*, *b* and *c*) and unit-cell volumes of mullite increased slightly after ZrO_2 addition, probably because the radius of Zr^{4+} (60.5 pm) is greater than that of Al^{3+} (53.5 pm). As Zr^{4+} replaced Al^{3+} in the aluminium oxide octahedral sites when forming a mullite solid solution, the lattice parameters (*a*, *b* and *c*) and unit-cell volume increased slightly. Therefore, the crystal structure of mullite was distorted after ZrO_2 addition, accelerating mass transfer and promoting the mullite reaction (Deng *et al.*, 2022).

Sintering behaviour

Figure 4 presents the bulk density and apparent porosity of the as-sintered ceramics with various amounts of ZrO_2 after sintering at various temperatures. With increasing sintering temperature, the bulk density and apparent porosity of the ceramics exhibited complex trends. The bulk density increased initially with increasing temperature from 1450°C to 1500°C, followed by a slight decrease from 1500°C to 1540°C, and then a sudden increase after sintering at 1560°C. The significant increase in bulk density after sintering at 1560℃ is attributed to the dense structure formed by the interleaving of rod-like mullite and the increasing amount of liquid phase filling the pores. In addition, the slight reduction in bulk density at 1500–1540°C is related to the expansion of secondary mullite formation and the phase transition of zirconia (i.e. *t*-ZrO_2 to *m*-ZrO_2) during cooling (Cui *et al.*, 2020; Lian *et al.*, 2021b). This phase transition resulted in volumetric expansion and decreased the bulk density.

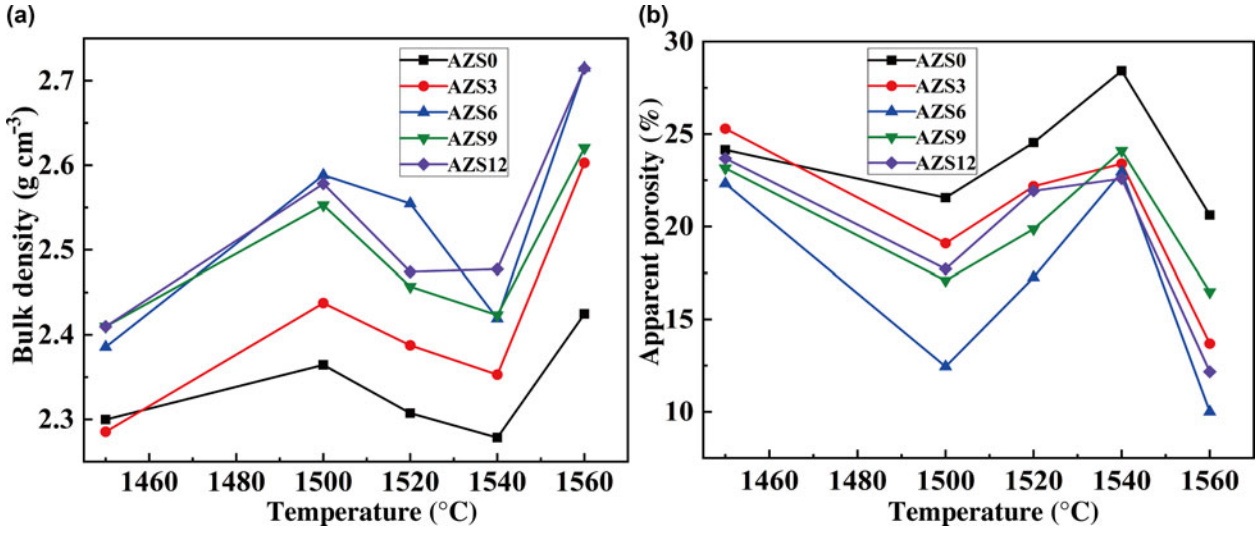

Fig. 4. (a) Bulk density and (b) apparent porosity of ceramics with various amounts of zirconia and after sintering at various temperatures.

https://doi.org/10.1180/clm.2022.25 Published online by Cambridge University Press

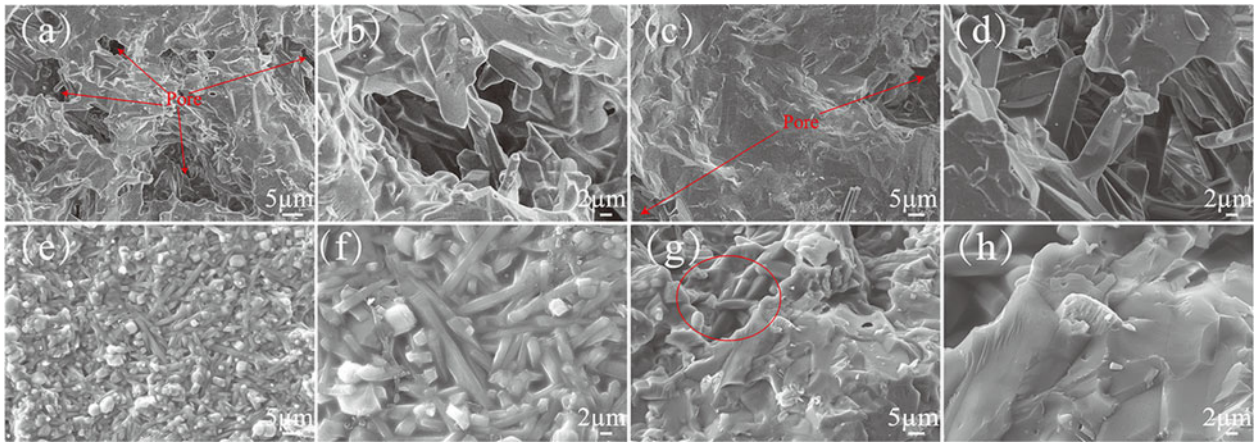

Fig. 5. SEM images of the fracture surfaces of ceramics after sintering at various temperatures: (a,b) AZS6 at 1500°C, (c,d) AZS6 at 1560°C, (e,f) AZS12 at 1500°C and (g,h) AZS12 at 1560°C.

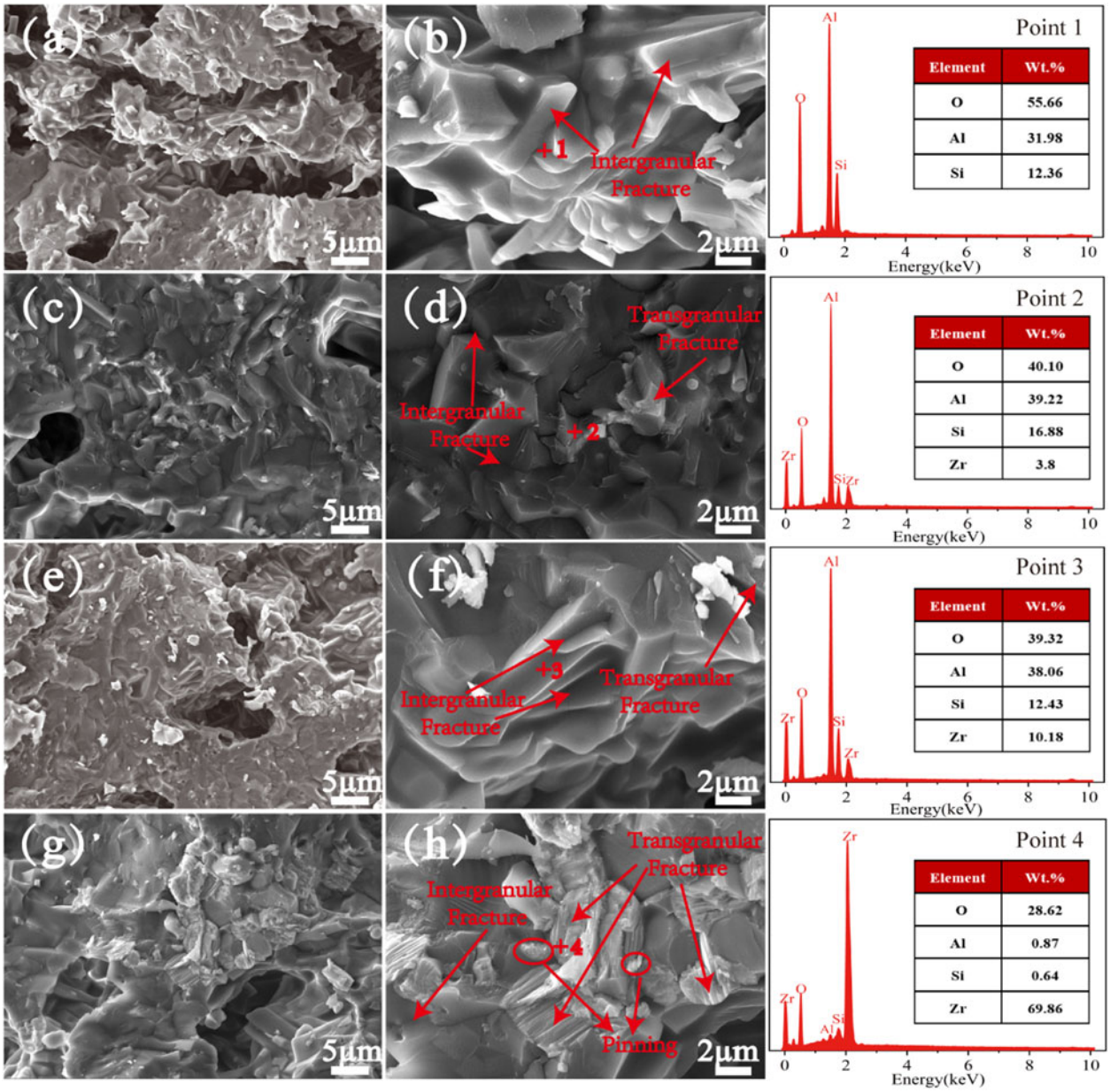

Fig. 6. SEM images and EDS analyses of ceramics with various amounts of ZrO_2 at 1560℃: (a,b) AZS0, (c,d) AZS3, (e,f) AZS9 and (g,h) AZS12.

https://doi.org/10.1180/clm.2022.25 Published online by Cambridge University Press

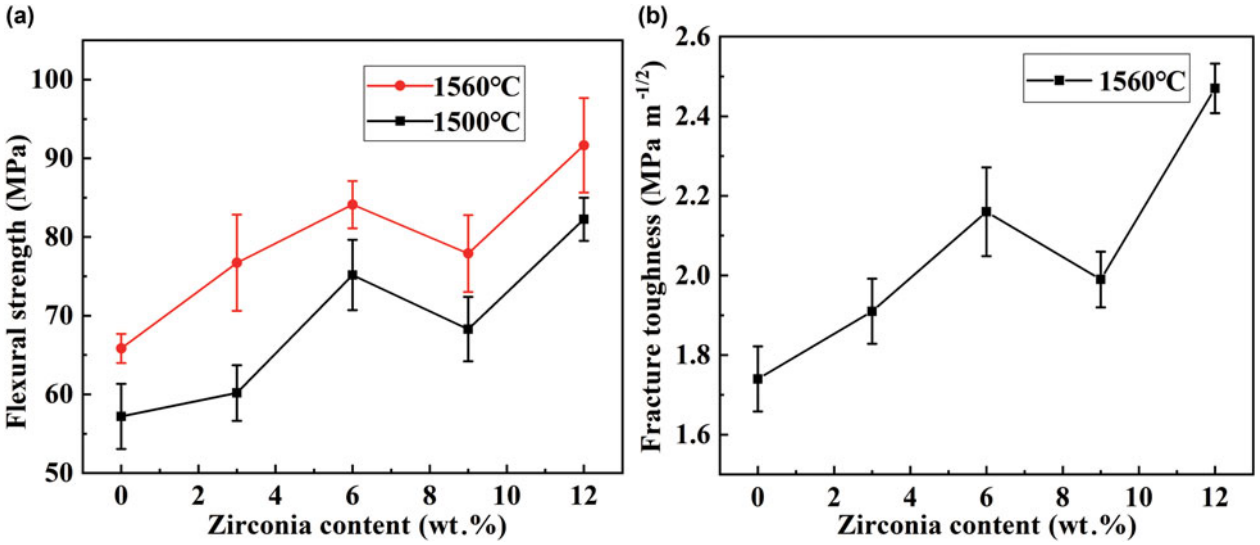

Fig. 7. Influence of ZrO_2 content on (a) flexural strength and (b) fracture toughness of the as-sintered ceramics.

Moreover, the bulk density of the ceramics increased significantly after the addition of zirconia. With increasing ZrO_2 content from 0 to 12 wt.%, the bulk density increased from 2.29 to 2.72 g cm^{-3} and the porosity decreased from 24.2% to 10.0%. The greatest bulk density of 2.72 g cm^{-3} was exhibited by AZS6 and AZS12 ceramics after sintering at 1560°C. In the case of AZS6, the liquid phase filled the pores, thereby increasing the bulk density (Fig. 5c,d). In the case of AZS12, excellent densification was achieved because rod-shaped mullite crystals were staggered and connected to form a dense network structure (Fig. 5g,h).

Microstructural analysis

Figure 5 shows the fracture surfaces of AZS6 and AZS12 ceramics after sintering at various temperatures. At 1500°C, pores are observed in the sample (Fig. 5a,b). The number of pores decreased after sintering at 1560°C (Fig. 5c,d), and columnar and rod-shaped mullite phases formed. Increasing sintering temperature also increased the proportion of the liquid phase, which filled the pores and grain boundaries. The presence of a liquid phase affected adversely the mechanical properties of the ceramics. The maximum bulk density of the AZS6 ceramic was 2.72 g cm^{-3}, while the flexural strength was only 84.1 MPa. This can be attributed to the introduction of zirconia, which distorted the lattice and increased the mass transfer, promoting the reaction between Al_2O_3 and SiO_2 (Feng *et al.*, 2022). In addition, rod-shaped mullite crystals were staggered and connected to form a dense network structure (red ellipse in Fig. 5g). The zirconia particles (brighter grains in Fig. 5) are distributed randomly at the grain boundaries, leading to a strong pinning effect (Fig. 5e,f). The pinning effect of zirconia grains hindered the movement of the grain boundaries, endowing the ceramics with excellent mechanical strength.

Figure 6 presents SEM images of the ceramics with various amounts of ZrO_2 after sintering at 1560°C. AZS0 exhibited a loose columnar microstructure (Fig. 6a,b). According to the EDS analysis of AZS0 (Fig. 6, point 1), the ratio of Al and Si atoms was ~3:1, suggesting mullite composition. The grain boundaries became obvious in the AZS3 ceramic after adding 3 wt.% ZrO_2 (Fig. 6c,d). When the ZrO_2 content increased to 9 wt.%, the structure of the as-sintered ceramic became loose (Fig. 6e,f), and the fracture modes of the ceramics were intergranular and transgranular (Lian *et al.*, 2021a). In addition, a small number of grains were pulled out on the fracture surface of the AZS12 ceramic, and the transgranular fracture was the main pathway for cracks (Fig. 6g,h). The transgranular fractures consumed a great amount of energy. Furthermore, the pinning effect of the zirconia particles (circular areas marked in Fig. 6h) deflected the grain boundaries and absorbed a great amount of fracture energy, improving the mechanical properties of the ceramics. Thus, the AZS12 ceramic exhibited the greatest strength (Fig. 7). Moreover, Fig. 6 (points 2 and 3) shows the EDS patterns of the AZS3 and AZS9 ceramics. The elements detected were Al, Si, O and Zr. The Zr content at point 3 in Fig. 6 (10.18%) was significantly greater than that at point 2 in Fig. 6 (3.8%), which is consistent with the greater contents of the zirconia phase with increasing ZrO_2 (Fig. 3b). The energy spectrum analysis of point 4 in Fig. 6 demonstrates that this is due to zirconia particles based on the proportion of Zr and O. The high Zr content may be related to the partial agglomeration of zirconia particles.

Mechanical characterization

Figure 7a shows the effect of ZrO_2 content on the flexural strength of ceramics after sintering at 1500℃ and 1560℃. The flexural strength increased with increasing sintering temperature, which is consistent with the trends for bulk density and apparent porosity (Fig. 4). With increasing ZrO_2 content, the connections between particles became tighter, increasing the strength and toughness of the ceramics. In addition, the occurrence of transgranular fractures also increased the strength of the as-sintered ceramics. Although the ceramics exhibit a combination of intergranular and transgranular fractures (Fig. 6), the *t*-ZrO_2/*m*-ZrO_2 ratio increased (Fig. 3b) with increasing ZrO_2 content, and the transgranular fractures became dominant (Lian *et al.*, 2021b). Therefore, when the ZrO_2 content increased to 12 wt.%, the flexural strength of the AZS12 ceramic reached a maximum value of 91.6 MPa and the fracture toughness reached a maximum value of 2.47 MPa m$^{-1/2}$, corresponding to increases of 37.6% in

https://doi.org/10.1180/clm.2022.25 Published online by Cambridge University Press

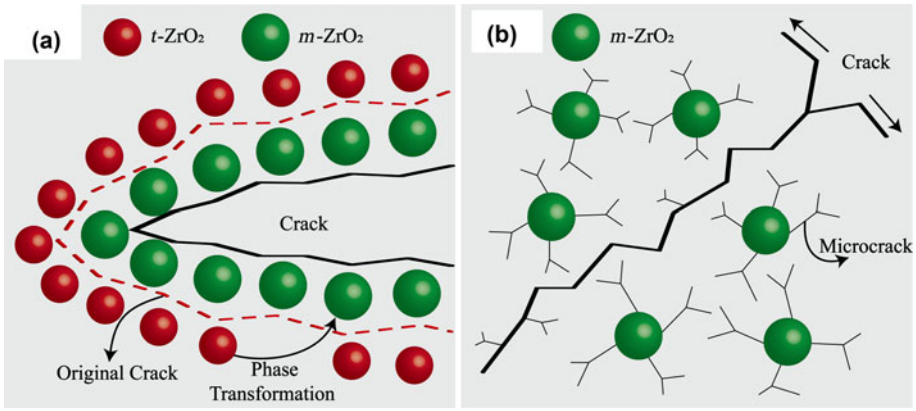

Fig. 8. Toughening mechanism of the zirconia additive: (a) phase-transformation toughening and (b) microcrack toughening.

flexural strength and 29.6% in fracture toughness (Fig. 7b). As confirmed using SEM analysis (Fig. 6g,h), the cracks passed through partially and destroyed the ZrO_2 particles, consuming large amounts of energy and increasing the mechanical strength of the as-sintered ceramics. The distribution of the secondary phase in the matrix also affected the flexural strength of the ceramics (Song *et al.*, 2018). Herein, zirconia particles were pinned at the grain boundaries, resulting in stress-induced transformation and microcrack toughening as the main mechanisms that improved the mechanical properties of the mullite composite ceramics.

Figure 8a presents a schematic illustration of ZrO_2-induced transformation toughening. The tetragonal ZrO_2 phase is transformed into a monoclinic phase through stress induction and exhibits volumetric expansion. The strain effect counteracts the influence of stress and absorbs energy, thereby alleviating stress concentration at the crack tip and improving the fracture toughness of the as-sintered ceramics. Figure 8b presents a schematic diagram of ZrO_2-induced microcrack toughening. The tetragonal phase in the matrix is transformed easily into the monoclinic phase, resulting in microcracks with increasing ZrO_2 grain size. As the size of the main crack begins to increase, the microcracks around the *m*-ZrO_2 particles absorb energy, reduce the stress concentration of the main crack, change the direction of crack propagation and, in turn, improve the mechanical properties of the as-sintered ceramics (Cui *et al.*, 2020). Therefore, the synergistic influence of phase-transformation toughening and microcrack toughening promotes the mechanical properties of the as-sintered ceramics.

Conclusions

The solid-state synthesis of mullite-based composite ceramics has been achieved using kaolin and Al_2O_3 as the starting materials. The sintering temperature (1450–1560°C) and ZrO_2 content affected the properties and morphologies of the composite ceramics significantly. In general, increasing sintering temperature increased the amount of the liquid phase, which was conducive to densification sintering. However, the bulk density decreased due to the expansion of secondary mullite and zirconia phase transformation in the temperature range 1500–1540°C. The interlocked structure was dominated by mullite, and the zirconia particles were dispersed at the grain boundaries, leading to a pinning effect. The AZS12 ceramic, sintered at 1560℃ for 3 h, demonstrated the greatest bulk density and flexural strength values of 2.72 g cm^{-3} and 91.6 MPa, respectively. The addition of ZrO_2 increased the flexural strength by ~37.6% due to the synergistic effect of zirconia phase transformation and ZrO_2 pinning at the grain boundaries. These results provide useful insights into the preparation of high-performance mullite-based composite ceramics using low-cost kaolin as a raw material.

Financial support. This work was supported by the National Natural Science Foundation of China (Grant No. 11872001), the Key Technologies R&D Program of Anhui Province of China (Grant No. 202104a05020033), the Foundation of State Key Laboratory of High-Efficiency Utilization of Coal and Green Chemical Engineering (Grant No. 2021-K19), the Anhui Provincial Major Science and Technology Special Program (Grant No. 18030901049), the School–Enterprise Cooperation Projects (Grant No. HX2021062279) and the College Students Innovation and Entrepreneurship Training Program (Grant No. S202110361147).

Supplementary material. To view supplementary material for this article, please visit https://doi.org/10.1180/clm.2022.25.

References

Alves H.P.A., Silva J.B., Campos L.F.A., Torres S.M., Dutra R.P.S. & Macedo D.A. (2016) Preparation of mullite based ceramics from clay–kaolin waste mixtures. *Ceramics International*, **42**, 19086–19090.

Aswad M.A., Alfatlawi S.H.A. & Saud A.N. (2021) Thermal decomposition and reaction sintering for synthesis of mullite–zirconia composite using kaolin, γ-alumina and zirconia. *Cerâmica*, **67**, 32–38.

Behera P.S. & Bhattacharyya S. (2020) Sintering and microstructural study of mullite prepared from kaolinite and reactive alumina: effect of MgO and TiO_2. *International Journal of Applied Ceramic Technology*, **18**, 81–90.

Bella M.L., Hamidouche M. & Gremillard L. (2021) Preparation of mullite–alumina composite by reaction sintering between Algerian kaolin and amorphous aluminum hydroxide. *Ceramics International*, **47**, 16208–16220.

Cui K., Zhang Y., Fu T., Wang J. & Zhang X. (2020) Toughening mechanism of mullite matrix composites: a review. *Coatings*, **10**, 672.

Deng L., Fu Z., Mingxing Z., Li H., Yao B., He J. *et al.* (2022) Crystallization, structure, and properties of TiO_2–ZrO_2 co-doped MgO–B_2O_3–Al_2O_3–SiO_2 glass–ceramics. *Journal of Non-Crystalline Solids*, **575**, 121217.

Feng M., Wu Y.-q., Ji G.-r., Zhou Y., Wang X.-j., Hao J.-y. *et al.* (2022) Sintering mechanism and properties of corundum–mullite duplex ceramic with MnO_2 addition. *Ceramics International*, **48**, 14237–14245.

Ji H., Fang M. & Huang Z. (2013) Effect of La_2O_3 additives on the strength and microstructure of mullite ceramics obtained from coal gangue and γ-Al_2O_3. *Ceramics International*, **39**, 6841–6846.

Jing Y., Deng X., Li J., Bai C. & Jiang W. (2014) Fabrication and properties of SiC/mullite composite porous ceramics. *Ceramics International*, **40**, 1329–1334.

Koyama T., Hayashi S. & Yasumori A. (1994) Preparation and characterization of mullite–zirconia composites from various starting materials. *Journal of the European Ceramic Society*, **14**, 295–302.

Koyama T., Hayashi S. & Yasumori A. (1996) Microstructure. and mechanical properties of mullite/zirconia composites prepared from alumina and zircon under various firing conditions. *Journal of the European Ceramic Society*, **16**, 231–237.

Kwon S.Y. & Jung I.-H. (2022) Thermodynamic assessment of the Al_2O_3–ZrO_2, CaO–Al_2O_3–ZrO_2, and Al_2O_3–SiO_2–ZrO_2 systems. *Ceramics International*, **48**, 5413–5427.

Li G., Ma H., Tian Y., Wang K., Zhou Y., Wu Y. *et al.* (2017) Feasible recycling of industrial waste coal gangue for preparation of mullite based ceramic proppant. *IOP Conference Series: Materials Science and Engineering*, **230**, 012020.

Li K., Ge S., Yuan G., Zhang H., Zhang J., He J. *et al.* (2021) Effects of V_2O_5 addition on the synthesis of columnar self-reinforced mullite porous ceramics. *Ceramics International*, **47**, 11240–11248.

Lian W., Liu Y., Wang W., Dong Y., Wang S., Zhu R. *et al.* (2021a) Effects of flake-shape and content of nano-mullite on mechanical properties and fracture process of corundum composite ceramics. *Journal of Asian Ceramic Societies*, **9**, 459–470.

Lian W., Liu Z., Zhu R., Wang W., Liu Y., Wang S. *et al.* (2021b) Effects of zirconium source and content on zirconia crystal form, microstructure and mechanical properties of ZTM ceramics. *Ceramics International*, **17**, 1026–1032.

Liu Y., Lian W., Su W., Luo J. & Wang L. (2019) Synthesis and mechanical properties of mullite ceramics with coal gangue and wastes refractory as raw materials. *International Journal of Applied Ceramic Technology*, **17**, 205–210.

Ma B.-y., Li Y., Cui S.-g. & Zhai Y.-c. (2010) Preparation and sintering properties of zirconia–mullite–corundum composites using fly ash and zircon. *Transactions of Nonferrous Metals Society of China*, **20**, 2331–2335.

Mahmood A.A., Gafur M.A. & Hoque M.E. (2017) Effect of MgO on the physical, mechanical and microstructural properties of ZTA–TiO_2 composites. *Materials Science and Engineering: A*, **707**, 118–124.

Mazzei A.C. & Rodrigues J.A. (2000) Alumina–mullite–zirconia composites obtained by reaction sintering. *Journal of Materials Science*, **35**, 2807–2814.

Miranzo P., Pena P., Moya J.S. & Deaza S. (1985) Multicomponent toughened ceramic materials obtained by reaction sintering. *Journal of Materials Science*, **20**, 2702–2710.

Mojumdar S., Prasad R. & Sun L. (2009) An introduction to thermodynamic modeling, thermal analysis and calorimetry. *Research Journal of Chemistry and Environment*, **13**, 86–103.

Peng L. & Qin S. (2019) Sintering behavior and technological properties of low-temperature porcelain tiles prepared using a lithium ore and silica crucible waste. *Minerals*, **9**, 731.

Prochazka S., Wallace J.S. & Glausen N. (1983) Microstructure of sintered mullite–zirconia composites. *Journal of the American Ceramic Society*, **66**, 125–127.

Ptáček P., Frajkorová F., Šoukal F. & Opravil T. (2014) Kinetics and mechanism of three stages of thermal transformation of kaolinite to metakaolinite. *Powder Technology*, **264**, 439–445.

Qian T., Zeng Y., Xiong X., Ye Z., Lun H., Hu J. *et al.* (2020) Corrosion behavior of Y_2O_3-doped mullite–$ZrSiO_4$ coatings applied on C/C–SiC composites in the presence of moisture at temperatures of 1373–1773 K. *Ceramics International*, **46**, 12861–12869.

Qin M., Tian Y.M., Hao H.L., Li G.M., Zhou Y. & Bai P.B. (2020) Effects of $CaCO_3$ additive on properties and microstructure of corundum- and mullite-based ceramic proppants. *International Journal of Applied Ceramic Technology*, **17**, 1026–1032.

Romero M., Padilla I., Contreras M. & López-Delgado A. (2021) Mullite-based ceramics from mining waste: a review. *Minerals – Basel*, **11**, 332.

Sahnoune F., Belhouchet H., Saheb N., Heraiz M., Chegaar M. & Goeuriot P. (2013) Phase transformation and sintering behaviour of mullite and mullite–zirconia composite materials. *Advances in Applied Ceramics*, **110**, 175–180.

Sainz M.A., Serrano F.J. & Amigo J.M. (2000) XRD microstructural analysis of mullites obtained from kaolinite–alumina mixtures. *Journal of the European Ceramic Society*, **20**, 403–412.

Sarker S., Mumu H.T., Al-Amin M., Zahangir Alam M. & Gafur M.A. (2022) Impacts of inclusion of additives on physical, microstructural, and mechanical properties of alumina and zirconia toughened alumina (ZTA) ceramic composite: a review. *Materials Today: Proceedings*, **62**, 2892–2918.

Schneider H., Schreuer J. & Hildmann B. (2008) Structure and properties of mullite – a review. *Journal of the European Ceramic Society*, **28**, 329–344.

Serragdj I., Harabi A., Kasrani S., Foughali L. & Karboua N. (2018) Effect of ZrO_2 additions on densification and mechanical properties of modified resistant porcelains using economic raw materials. *Journal of the Australian Ceramic Society*, **55**, 489–499.

Sistani P.B., Kiani-Rashid A. & Beidokhti S.M. (2019) Microstructural and diametral tensile strength evaluation of the zirconia–mullite composite. *Ceramics International*, **45**, 7127–7136.

Song Y., Zhu D., Liang J. & Zhang X. (2018) Enhanced mechanical properties of 3 mol% Y_2O_3 stabilized tetragonal ZrO_2 incorporating tourmaline particles. *Ceramics International*, **44**, 15550–15556.

Vyazovkin S., Burnham A.K., Criado J.M., Pérez-Maqueda L.A., Popescu C. & Sbirrazzuoli N. (2011) ICTAC Kinetics Committee recommendations for performing kinetic computations on thermal analysis data. *Thermochimica Acta*, **520**, 1–19.

Weinberg A.V., Goeuriot D., Poirier J., Varona C. & Chaucherie X. (2021) Mullite–zirconia composite for the bonding phase of refractory bricks in hazardous waste incineration rotary kiln. *Journal of the European Ceramic Society*, **41**, 995–1002.

Wu J., Ding C., Xu X. & Chen L. (2021a) Preparation and thermal stability investigation of Al_2O_3–mullite–ZrO_2–SiC composite ceramics for solar thermal transmission pipelines. *Ceramics International*, **47**, 10672–10678.

Wu J., Ding C., Xu X., Liu Y. & Wang Y. (2021b) Microstructure and performances of corundum–mullite composite ceramics for heat transmission pipelines: effects of Ho_2O_3 additive content. *Ceramics International*, **47**, 34794–34801.

Wu J., Ding C., Xu X., Zhou S., Zhou Y. & Zhang Q. (2021c) Microstructure and performances of Gd_2O_3-added corundum–mullite ceramic composites for concentrated solar power applications. *Ceramics International*, **47**, 17177–17185.

Wu J., Hu C., Xu X., Ma X. & Zhang Y. (2016) Preparation and performance study of mullite/Al_2O_3 composite ceramics for solar thermal transmission pipeline. *International Journal of Applied Ceramic Technology*, **13**, 1017–1023.

Yuan Q.-M., Tan J.-Q. & Jin Z.-G. (1986) Preparation and properties of zirconia-toughened mullite ceramics. *Journal of the American Ceramic Society*, **69**, 265–267.

Yuan W., Kuang J., Huang Z. & Yu M. (2022) Effect of aluminum source on the kinetics and mechanism of mullite preparation from kaolinite. *Chemical Physics Letters*, **787**, 139242–139248.

Yu H., Chen Y., Guo X., Luo L., Li J., Li W. *et al.* (2018) Study on mechanical properties of hot pressing sintered mullite–ZrO_2 composites with finite element method. *Ceramics International*, **44**, 7509–7514.

Zhang B., Ma J., Ye J., Jin Y., Yang C., Ding J. *et al.* (2019) Ultra-low cost porous mullite ceramics with excellent dielectric properties and low thermal conductivity fabricated from kaolin for radome applications. *Ceramics International*, **45**, 18865–18870.

https://doi.org/10.1180/clm.2022.25 Published online by Cambridge University Press